Geol. Mag. **142** (*3*), *2005, pp. 255–268.* *© 2005 Cambridge University Press*
doi:10.1017/S0016756805000506 *Printed in the United Kingdom*

Depositional constraints and age of metamorphism in southern India: U–Pb chemical (EMPA) and isotopic (SIMS) ages from the Trivandrum Block

M. SANTOSH*, A. S. COLLINS†, T. MORIMOTO* & K. YOKOYAMA‡

*Faculty of Science, Kochi University, Akebono-cho 2-5-1, Kochi 780-8520, Japan
†Discipline of Geology & Geophysics and Tectonics Special Research Centre, School of Earth & Environmental Sciences, The University of Adelaide, Adelaide, SA 5005, Australia
‡Department of Geology, National Science Museum, 3-23-1, Hyakunin-cho, Shinjuku-ku, Tokyo 169-0073, Japan

---

(*Received* 2 February 2004; *accepted* 14 January 2005)

Abstract – We report U–Pb electron microprobe (zircon and monazite) and Secondary Ion Mass Spectrometry (SIMS) U–Pb (zircon) ages from a granulite-facies metapelite and a garnet–biotite gneiss from Chittikara, a classic locality within the Trivandrum Block of southern India. The majority of the electron-microprobe data on zircons from the metapelite define apparent ages between 1500 and 2500 Ma with a prominent peak at 2109 ± 22 Ma, although some of the cores are as old as 3070 Ma. Zircon grains with multiple age zoning are also detected with 2500–3700 Ma cores, 1380–1520 mantles and 530–600 Ma outer rims. Some homogeneous and rounded zircon cores yielded late Neoproterozoic ages that suggest that deposition within the Trivandrum Block belt was younger than 610 Ma. The outermost rims of these grains are characterized by early Cambrian ages suggesting metamorphic overgrowth at this time. The apparent ages of monazite grains from this locality reveal multiple provenance and polyphase metamorphic history, similar to those of the zircons. In a typical case, Palaeoproterozoic cores (1759–1967 Ma) are enveloped by late Neoproterozoic rims (562–563 Ma), which in turn are mantled by an outermost thin Cambrian rim (∼ 515 Ma). PbO v. ThO_2^* plots for monazites define broad isochrons, with cores indicating a rather imprecise age of 1913 ± 260 Ma (MSWD = 0.80) and late Neoproterozoic/Cambrian cores as well as thin rims yielding a well-defined isochron with an age of 557 ± 19 Ma (MSWD = 0.82). SIMS U–Pb isotopic data on zircons from the garnet–biotite gneiss yield a combined core/rim imprecise discordia line between 2106 ± 37 Ma and 524 ± 150 Ma. The data indicate Palaeoproterozoic zircon formation with later partial or non-uniform Pb loss during the late Neoproterozoic/Cambrian tectonothermal event. The combined electron probe and SIMS data from the metapelite and garnet–biotite gneiss at Chittikara indicate that the older zircons preserved in the finer-grained metapelite protolith have heterogeneous detrital sources, whereas the more arenaceous protolith of the garnet–biotite gniess was sourced from a single-aged terrane. Our data suggest that the metasedimentary belts in southern India may have formed part of an extensive late Neoproterozoic sedimentary basin during the final amalgamation of the Gondwana supercontinent.

Keywords: electron microprobe dating, monazite, Southern Granulite Terrane, India, SHRIMP, zircon.

1. Introduction

Microprobe U–Pb geochronological techniques are particularly useful in resolving the often complex geological evolution of high-grade rocks, as these techniques allow discrete domains of minerals to be dated by either chemical (e.g. electron microprobe analysis, EMPA) or isotopic (e.g. secondary ion mass spectrometry, SIMS) methods. Thermally robust minerals, such as zircon and monazite, within granulite-facies rocks often preserve cores that contain information as to the nature and age of the protolith. In metasedimentary rocks, these cores can be used to constrain the depositional age of the protolith and shed light on the source region of the original sediment (e.g. Collins *et al.* 2003). In this paper, we analyse zircons and monazites from metasedimentary rocks in southern India to constrain their age, examine possible provenance regions and address the implications of these data for the amalgamation of this part of Gondwana.

The southern part of the high-grade metamorphic terrain of southern India comprises a vast supracrustal belt originally known as the Kerala Khondalite Belt (Chacko, Ravindra Kumar & Newton, 1987), but more recently referred to as the Trivandrum Block (Santosh, 1996) (Fig. 1), which contains a sequence of psammitic, psammopelitic and pelitic metasedimentary rocks and local orthogneisses that have been subjected to high-grade metamorphism under granulite-facies conditions. The dominant rock types in this belt are garnet- and sillimanite-bearing metapelitic granulites (khondalites) with or without cordierite, spinel

---

† Author for correspondence: alan.collins@adelaide.edu.au

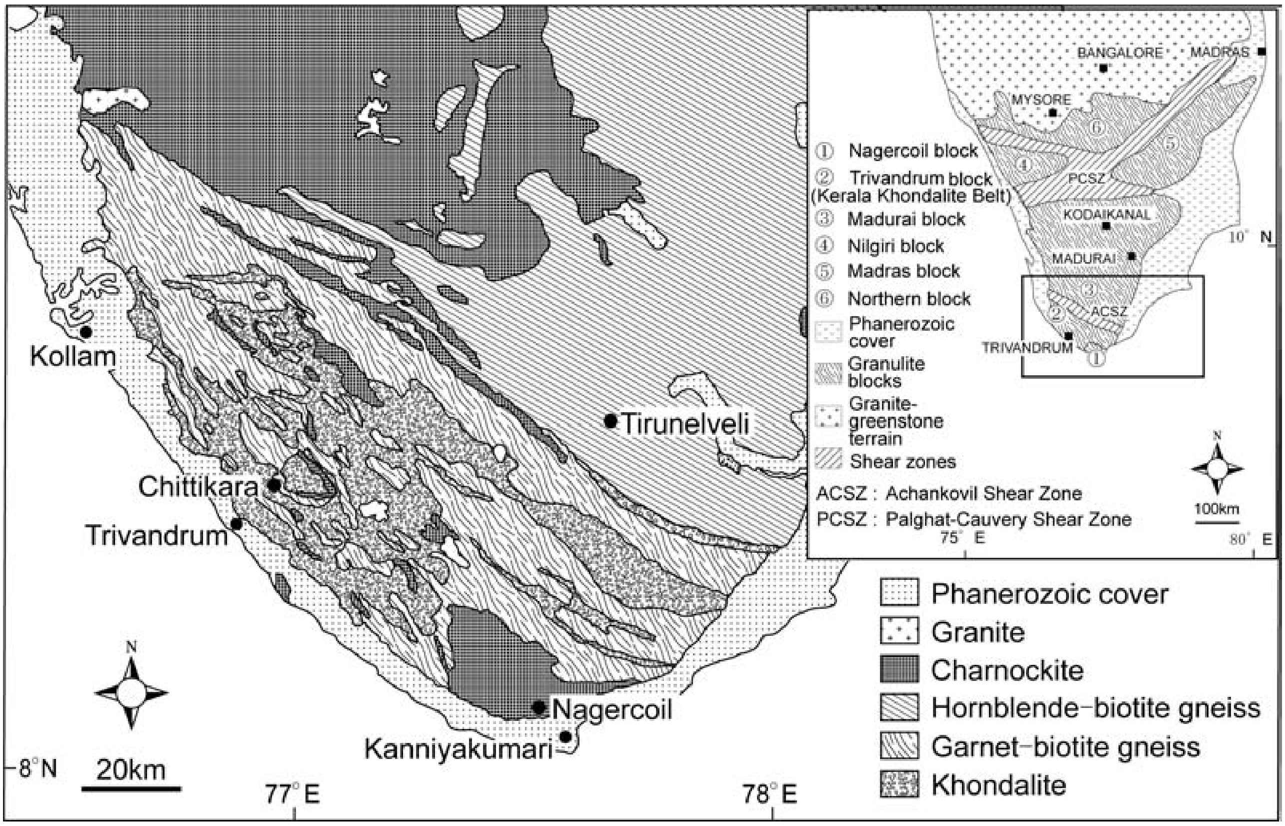
① Nagercoil block
② Trivandrum block (Kerala Khondalite Belt)
③ Madurai block
④ Nilgiri block
⑤ Madras block
⑥ Northern block
Phanerozoic cover
Granulite blocks
Granite-greenstone terrain
Shear zones
ACSZ : Achankovil Shear Zone
PCSZ : Palghat-Cauvery Shear Zone
BANGALORE
MADRAS
MYSORE
PCSZ
KODAIKANAL
MADURAI
ACSZ
TRIVANDRUM
10° N
75° E
80° E
N
100km
Kollam
Tirunelveli
Chittikara
Trivandrum
Nagercoil
Kanniyakumari
N
8°N
20km
77° E
78° E
Phanerozoic cover
Granite
Charnockite
Hornblende-biotite gneiss
Garnet-biotite gneiss
Khondalite

Figure 1. Geological map of southern Kerala and a part of Tamil Nadu showing the Trivandrum Block and location of the present study area (Chittikara). The inset map shows the tectonic framework of southern India.

and graphite. The metapelites are intercalated with varying amounts of garnet-biotite gneiss (leptynite), garnet- and orthopyroxene-bearing anhydrous granulites (charnockites and enderbites) and subordinate bands, boudins and lenses of pyroxene granulite and calc-silicate rocks. High-grade metamorphism and granulite formation in the Trivandrum Block are linked to the late Neoproterozoic–Cambrian tectonothermal event associated with the birth of the Gondwana supercontinent (Stern, 1994; Meert & Van der Voo, 1997; Collins & Windley, 2002; Braun & Kriegsman, 2003; Meert, 2003; Santosh *et al*. 2003; Collins & Pisarevsky, 2005).

The Trivandrum Block has been the focus of various geological, petrological, isotopic and geochronological investigations for nearly two decades (for a recent review, see Braun & Kriegsman, 2003). Much research has been focused on cordierite, sillimanite and spinel-bearing metapelite assemblages commonly found in this terrain that provide important clues to the pressure–temperature conditions and exhumation history of the region (e.g. Santosh, 1987; Santosh, Jackson & Harris, 1993; Nandakumar & Harley, 2000; Cenki, Kriegsman & Braun, 2002). In this context, the Chittikara Quarry [N08° 36′ 31.8″ E76° 53′ 54.6″] located about 15 km north of Trivandrum (Fig. 1) has attracted particular interest (Santosh, Jackson & Harris, 1993; Santosh & Wada, 1993*a*,*b*; Morimoto *et al*. 2004).

In this study, we report results from U–Th–Pb age dating of zircon and monazite from the Chittikara metapelite and garnet–biotite gneiss, using both electron probe microanalysis (EPMA) and Secondary Ion Mass Spectrometry (SIMS) techniques, in order to investigate the source characteristics of the metasedimentary gneisses and attempt to date the metamorphic history of this key region of southern India.

2. Geological background, petrology and *P*–*T* conditions

At Chittikara, a large active quarry provides fresh exposures of granulite-facies metapelites. The rocks predominantly comprise garnet–sillimanite–spinel–cordierite-bearing metapelites that occur as bands of varying width ranging from a few centimetres to more than 2 m intercalated within garnet- and biotite-bearing felsic gneisses. They are deformed into tight isoclinal folds and rootless intrafolial folds. Cordierite occurs along the compositional layers and also as large purple crystals. Graphite occurs in a variety of associations in this locality. Thin flakes and fine disseminated graphite within the metapelite bands represent the conversion of biogenic material trapped within host sediments during high-grade metamorphism as indicated by their carbon isotope composition (Santosh & Wada, 1993*a*). Coarse flakes and flaky aggregates of graphite occurring with patches, veins and late shears/fractures have isotopic compositions characterized by enrichment in heavier carbon indicating precipitation from magmatically derived CO_2-rich fluids (Santosh & Wada, 1993*b*).

The most common assemblage of the Chittikara metapelite is Grt + Sil + Crd + Spl + Kfs + Bt + Qtz + Pl + Gr with accessory zircon and monazite (mineral abbreviations are after Kretz, 1983). Aluminous melanosomes are characterized by the assemblage Grt + Sil + Crd + Bt + Kfs ± Spl ± Ilm ± Gr, and alternate with felsic leucosomes containing mostly Kfs + Qtz + Bt + Pl. Zircon (100–250 μm) and monazite (up to 300 μm) occur mostly as inclusions within garnet and cordierite. Plagioclase and K-feldspar also sometimes carry zircon and monazite inclusions. Rarely, zircon and monazite also form inclusions within spinel and sillimanite.

Morimoto *et al.* (2004) identified a series of mineral reaction textures in the Chittikara metapelite that they used to calculate metamorphic temperatures between 850 °C and 1000 °C at pressures of ~7 kbar. Based on textural mineral reaction and pressure–temperature data, Morimoto *et al.* (2004) proposed a P–T path for the metapelite that is characterized by an initial isobaric component, followed by a steep and virtually isothermal decompression from 7 kbar down to 4 kbar.

3. Sample preparation and analytical techniques

The theoretical concepts of EPMA dating technique followed in this study and the equations for age computations are described in detail in Suzuki & Adachi (1991, 1992), Montel *et al.* (1996) and Santosh *et al.* (2003).

Fresh rock chips were crushed into fine fractions in a stainless-steel stamp mill. Powdered samples (< 100 μm mesh size) were cleaned using water to remove the dust particles, and then dried in an oven. The magnetic minerals were then removed using a hand magnet. Heavy fractions were separated by methylene iodide, mounted on glass slides using epoxy resin, and diamond polished. Polished grain mounts were used for the study of grain characteristics and EPMA analyses. Samples for SIMS analysis were mounted in epoxy resin and coated with gold. They were imaged using a cathodoluminescence (CL) detector fitted to a Phillips XL30 scanning electron microscope at a working distance of 15 mm and using an accelerating voltage of 10 kV. The resulting images highlight distortions in the crystal lattice (Stevens Kalceff *et al.* 2000) that are related to trace-element distribution and/or radiation damage (Rubatto & Gebauer, 2000).

Chemical analyses were made using an electron microprobe (JEOL JXA-8800) at the National Science Museum, Tokyo, Japan, with a 15 kV accelerating voltage, 0.5 μA probe current (0.2 μA for monazite), 2 μm probe diameter and 200–300 seconds counting time for U, Th and Pb. PRZ corrections (modified ZAF) were applied for the analyses. U, Th and Pb standards were synthesized γ-UO_3, ThO_2 and natural crocoite ($PbCrO_4$), respectively. Natural and synthesized minerals were used as standards for other elements. Seven elements (Si, Zr, Y, Hf, U, Th, Pb) for zircon and 14 elements (P, Si, La, Ce, Pr, Nd, Sm, Gd, Dy, Y, U, Th, Pb, Ca) for monazite were analysed. UMα, ThMα, PbMα lines were used in the U, Th and Pb analyses, respectively, and the spectral interferences of the ThMζ, YLχ and ZrLγ lines with the PbMα line, and the ThMβ line with the UMα line were corrected. Age calibrations were performed by comparing data obtained from zircons and monazites by EPMA dating with those generated by the SIMS technique using the Sensitive High-mass Resolution Ion Microprobe (SHRIMP). Apart from minor shifts due to machine drift and standard conditions, the ages obtained from both techniques were found to be within error. Internal age standards used were a 994 ± 5 Ma zircon from an Antarctic rock analysed by SHRIMP and a 3019 ± 4 Ma monazite from Australia. The latter is the SHRIMP age of the coexisting zircon. Both internal standards were routinely analysed before and after the analyses of unknown samples.

The error (1-sigma confidence level) of age measurements for each zircon analysis includes instrumental counting statistics only, and is approximately 3 % at PbO = 0.05 wt % to *c.* 10 % at PbO = 0.02 wt % level. Least-squares fitting was applied to calculate the ages by linear regression, assuming each dataset belongs to a single zircon-forming event. EPMA zircon analyses are less precise than EPMA monazite analyses because of the low levels of Pb commonly found in zircon, and may be less accurate due to the greater likelihood of undetectable common Pb in the zircon grains.

Zircon U–Th–Pb isotopic data were collected using the SHRIMP II based in the John de Laeter Centre of Mass Spectrometry, Perth, Western Australia. The sensitivity for Pb isotopes in zircon using SHRIMP II was ~18 cps/ppm/nA, the primary beam current was 2.5–3.0 nA and mass resolution was ~5000. Correction of measured isotopic ratios for common Pb was based on the measured ^{204}Pb in each sample and often represented a < 1 % correction to the ^{206}Pb counts (see %com. ^{206}Pb in Table 3). The common Pb component, being largely surface contaminant, was modelled on the composition of Broken Hill ore Pb (Cooper, Reynolds & Richards, 1969).

Pb/U isotopic ratios were corrected for instrumental inter-element discrimination using the observed covariation between Pb^+/U^+ and UO^+/U^+ (Hinthorne *et al.* 1979; Compston, Williams & Meyer, 1984) determined from interspersed analyses of the Perth standard zircon CZ3. CZ3 is a single zircon megacryst from Sri Lanka with an age of 564 Ma and $^{206}Pb/^{238}U = 0.0914$ (Nelson, 1997).

4. Results

U–Pb electron probe analytical data on zircons and monazites from the metapelite sample along with the calculated ages and errors are given in Tables 1 and 2. Where PbO content in zircon is too low (< 0.02 ppm) to obtain U–Th–Pb age within reasonable error level, these have been discarded from age calculations. SHRIMP U–Th–Pb isotopic data are provided in Table 3.

4.a. Morphology, backscattered electron and cathodoluminescence response

Zircon and monazite are common accessories in the Chittikara metapelites. Zircon grains show a size range of 100–250 µm and exhibit different grain morphologies ranging from euhedral crystals to subhedral, sub-rounded and rounded (Fig. 2). The relatively brighter portions under backscattered electron imaging (BEI) indicate chemically homogeneous domains. Oscillatory zoning is displayed by some grain cores (Fig. 2a, b, d, g, h). The cores are either subhedral (Fig. 2a, g, h) or sub-rounded (Fig. 2b). These detrital cores are mantled by multiple rims of various thicknesses indicating formation of either successive overgrowths or complex diffusion/recrystallization fronts during successive tectonothermal regimes. Some zircons show sub-rounded or rounded grain margins with homogeneous cores that do not display visible growth zones (Fig. 2c), although a younger mantle envelops the cores. The rounding of the grain cores suggests that they experienced sedimentary transport, but may in part be due to diffusion-driven solid-state recrystallization fronts (e.g. Hoskin & Black, 2000).

Backscattered electron images of representative monazite grains from Chittikara are shown in Figure 3. Monazite grains from the metapelite range in size from 100 to 300 µm. The grain outlines are subhedral to anhedral, although they incorporate core portions with variable morphology. Thus, rounded to sub-rounded cores (Fig. 3a, b, e) as well as subhedral cores (Fig. 3c, g) are present. In some cases, apparent oscillatory zoning occurs (e.g. Fig. 3d, g). However, most of the zoning patterns in the Chittikara monazites are of successive irregular mantles overgrown on variable cores. Some of the intermediate zones in such cases resemble diffusion/recrystallization fronts between the inner core and outer mantle (e.g. Fig. 3e). From grain morphology and internal growth patterns of monazites in Chittikara, it can be inferred that while some grains formed from a single thermal event, others possess the history of multiple source regions, more than one tectonothermal regime or subsequent alteration by hydrothermal alteration.

4.b. Age data

Figure 2 shows the age values in the various zones within zircon grains computed from electron probe data. In general, there is a trend of decreasing age from core to rim of individual grains, except in cases where there has been local metamictization or probable diffusion induced by high-temperature fluids propagating through cracks such as the isolated younger core values in the grain shown in Figure 2d. Zircon core analyses indicate dates back to 3070 Ma (Table 1, Fig. 2f) although the majority of data provide apparent ages between 1500 and 2500 Ma with a prominent peak at 2109 ± 22 Ma (Fig. 4). The sub-rounded zircon in Figure 2e–f has the oldest relict core identified in this study with an age range between 2500–3070 Ma. This grain incorporates three tiny core fragments (seen as the relatively brightest portions in the BEI image, Fig. 2e), which are enveloped by a thick zone with ages ranging from 1380 to 1520 Ma (Table 1, Fig. 2f). This is in turn mantled by a thin rim with apparent ages in the range of 530 to 600 Ma. This grain clearly indicates the multiple growth history of zircons in the Chittikara metapelites and shows that some grains were originally derived from Archaean sources. Importantly, some of the zircons are characterized by homogeneous and rounded cores with late Neoproterozoic ages (e.g. Fig. 2c). This may indicate that deposition within the Trivandrum Block was as young as, or later than, 610 Ma. These grains have an outermost rim with early Cambrian ages, indicating metamorphic overgrowth at this time. Isotopic analysis and more textural work is required to further confirm a Neoproterozoic depositional age.

The cores of monazites in Figure 3a–b show Palaeo-Mesoproterozoic ages and are mantled by late Neoproterozoic/Cambrian rims. The grain core shown in Figure 3c preserves ~635–590 Ma apparent ages and is rimmed by monazite with apparent ages > 25 Ma younger. The relatively homogeneous grain in Figure 3d shows no marked age variation and does not display a pronounced compositional rim. We suggest that this grain formed, or was chemically reset, during a single thermal event at 557–579 Ma. The grains shown in Figure 3e–h clearly bring out two contrasting monazite growth periods. The grain shown in Figure 3e and f has a Palaeo-Mesoproterozoic dark core (1759–1967 Ma, zone ‘a’ in the sketch), which is mantled by a late Neoproterozoic rim (562–563 Ma, zones ‘b’ and ‘c’ in the sketch). An outermost thin Cambrian rim (515 Ma, zone ‘d’ in the sketch) envelops the grain. The highly irregular boundaries between some of the compositional/apparent age zones in Figure 3 (e.g. between zones a and b in Fig. 3f) suggest that the rims formed, at least partially, by chemical transformation of pre-existing monazite by either: (1) diffusive element advection; (2) diffusion-driven solid-state recrystallization; or (3) dissolution/re-precipitation. The sharply defined outer late Neoproterozoic and Cambrian rims probably represent newly precipitated monazite on a dissolution surface (e.g. Fig 3f, zones c and d; Fig 3h, zone c). Similar complex rims to monazites are widely reported and have been explained in terms

Table 1. Electron probe analytical data on zircons from Chittikara metapelite

Grain no.	UO_2 (wt %)	ThO_2 (wt %)	PbO (wt %)	Count error PbO (%)	Age (Ma)	Error age (Ma)	ThO_2^* (wt %)
CHT2-1A-b	0.056	0.031	0.022	9.354	2060	226	0.247
	0.101	0.059	0.046	4.549	2280	127	0.456
	0.730	0.04	0.267	0.785	2120	19	2.863
	0.949	0.072	0.327	0.642	2010	15	3.696
	0.802	0.043	0.285	0.737	2070	17	3.126
	0.276	0.012	0.076	2.766	1690	51	1.028
	0.073	0.053	0.033	6.427	2200	171	0.337
	0.199	0.192	0.092	2.288	2150	60	0.966
	0.068	0.042	0.031	6.701	2280	187	0.310
	0.057	0.04	0.025	8.363	2170	219	0.262
	0.133	0.083	0.060	3.529	2230	95	0.604
	0.242	0.011	0.081	2.604	1970	58	0.930
CHT2-1A-d	0.075	0.026	0.031	6.679	2210	175	0.321
	0.152	0.013	0.032	6.484	1350	92	0.553
	0.208	0.187	0.079	2.654	1870	57	0.966
	0.137	0.12	0.060	3.499	2100	88	0.649
	0.106	0.069	0.045	4.710	2100	117	0.480
	0.114	0.069	0.042	4.968	1920	109	0.501
	0.081	0.04	0.036	5.832	2260	159	0.359
	0.144	0.009	0.029	7.309	1290	99	0.517
	0.263	0.032	0.084	2.495	1880	52	1.022
	0.385	0.052	0.133	1.582	1990	36	1.517
CHT2-1A-e	0.215	0.044	0.020	10.627	610	65	0.761
	0.285	0.025	0.021	10.061	510	52	0.969
	0.253	0.012	0.023	8.958	640	58	0.857
CHT2-1A-f	0.276	0.024	0.022	9.715	540	53	0.940
CHT2-1A-g	0.093	0.01	0.029	7.317	1840	149	0.357
	0.120	0	0.025	8.407	1350	119	0.427
CHT2-1A-h	0.097	0	0.035	6.027	2110	145	0.375
CHT2-1A-i	0.073	0.05	0.026	8.147	1830	169	0.322
CHT2-1A-j	0.102	0	0.028	7.598	1690	139	0.375
	0.102	0.045	0.032	6.464	1760	126	0.423
CHT2-1A-l	0.077	0.037	0.023	9.084	1660	166	0.320
	0.240	0.131	0.101	2.084	2150	53	1.062
	0.169	0.051	0.045	4.704	1550	79	0.663
	0.366	0.011	0.028	7.466	540	41	1.224
	0.217	0.105	0.091	2.317	2160	59	0.950
	0.123	0.049	0.033	6.305	1550	106	0.495
	0.259	0.054	0.074	2.852	1670	52	1.005
	0.162	0.082	0.057	3.685	1880	79	0.691
	0.167	0.041	0.047	4.429	1660	80	0.654
	0.242	0.135	0.081	2.604	1780	52	1.034
	0.258	0	0.021	10.225	570	59	0.857
CHT2-1A-m	0.032	0.007	0.021	9.931	1980	280	0.128
	0.218	0.045	0.060	3.501	1630	62	0.843
	0.241	0.02	0.020	10.557	570	61	0.819
	0.176	0.033	0.053	3.994	1750	77	0.686
	0.216	0.119	0.090	2.333	2130	59	0.956
	0.118	0.032	0.041	5.185	1930	113	0.479
	0.035	0.009	0.023	9.317	2010	263	0.142
	0.106	0.048	0.047	4.503	2270	123	0.465
	0.299	0	0.026	8.076	610	50	0.997
CHT2-1A-n	0.117	0	0.024	8.766	1330	122	0.416
	0.157	0	0.022	9.518	960	93	0.539
	0.118	0	0.023	9.154	1280	122	0.417
	0.142	0.007	0.020	10.870	920	102	0.492
CHT2-1A-o	0.109	0.055	0.057	3.659	2570	121	0.501
	0.113	0.05	0.057	3.680	2510	117	0.510
	0.119	0.045	0.080	2.635	3070	116	0.574
	0.118	0.062	0.069	3.035	2760	113	0.559
	0.481	0.052	0.037	5.722	530	31	0.444
	0.278	0	0.024	8.750	600	53	0.460
	0.122	0.056	0.064	3.293	2570	108	0.556
	0.071	0.026	0.042	4.970	2840	190	0.331
	0.081	0.029	0.021	9.807	1520	161	0.323
	0.110	0.051	0.056	3.729	2530	120	0.499
	0.110	0.06	0.064	3.287	2740	120	0.521
	0.108	0.074	0.070	2.990	2890	122	0.541
	0.069	0.032	0.041	5.131	2800	193	0.326
	0.086	0.025	0.022	9.464	1510	153	0.337
	0.116	0.06	0.059	3.564	2500	113	0.530
	0.082	0.02	0.020	11.346	1380	166	0.311

Table 2. Electron probe analytical data on monazites from Chittikara metapelite

Grain no.	UO_2 (wt %)	ThO_2 (wt %)	PbO (wt %)	Count error PbO (%)	Age (Ma)	Error age (Ma)	ThO_2^* (wt %)
CHT2-1A-1	0.780	3.470	0.279	1.399	1053	16	6.171
	0.352	12.490	0.327	1.193	564	7	13.659
	0.398	4.300	0.125	3.117	526	17	5.618
	0.558	7.990	0.218	1.788	523	10	9.837
	0.837	12.280	0.337	1.156	529	6	15.053
	0.513	20.730	0.537	0.726	565	4	22.433
	1.325	5.980	0.257	1.518	583	9	10.387
	0.636	4.590	0.171	2.283	600	14	6.709
	0.592	20.060	0.508	0.768	544	4	22.022
	0.528	19.730	0.508	0.768	557	4	21.482
	0.454	5.370	0.153	2.544	526	14	6.873
	0.471	4.020	0.416	0.938	1659	18	5.748
	0.849	2.490	0.365	1.067	1514	20	5.559
	1.363	6.080	0.269	1.449	597	9	10.619
	0.774	3.670	0.160	2.444	601	15	6.249
	0.383	4.780	0.129	3.025	504	15	6.046
CHT2-1A-2	0.331	3.860	0.101	3.872	480	19	4.953
	0.636	10.580	0.285	1.367	530	7	12.686
	0.887	14.510	0.394	0.989	533	5	17.448
	0.666	7.820	0.223	1.752	524	9	10.024
	0.515	1.250	0.071	5.513	563	32	2.960
	0.306	3.570	0.093	4.203	478	20	4.581
	0.510	1.540	0.074	5.238	543	29	3.231
CHT2-1A-3	1.491	4.720	0.252	1.547	612	10	9.692
	0.322	16.760	0.417	0.935	552	5	17.827
	0.304	16.360	0.416	0.938	564	5	17.370
	0.322	17.380	0.434	0.898	555	5	18.448
	1.578	4.880	0.264	1.479	612	9	10.141
CHT2-1A-3	1.501	4.760	0.250	1.559	603	10	9.759
	1.504	4.580	0.259	1.508	633	10	9.604
	0.326	18.670	0.467	0.834	558	5	19.752
	0.814	12.210	0.334	1.167	529	6	14.905
	0.229	10.620	0.271	1.437	562	8	11.381
	1.481	4.750	0.244	1.600	593	10	9.679
	1.578	4.890	0.267	1.461	619	9	10.153
CHT2-1A-4	0.526	14.510	0.396	0.984	574	6	16.258
	0.263	16.190	0.410	0.951	566	6	17.062
	0.329	15.930	0.410	0.950	568	6	17.023
	0.315	13.900	0.354	1.102	558	6	14.947
	0.322	13.740	0.362	1.078	575	6	14.810
	0.264	13.840	0.362	1.079	579	6	14.717
	0.390	14.900	0.385	1.013	560	6	16.194
	0.330	16.750	0.422	0.925	557	5	17.845
	0.299	16.030	0.407	0.958	564	6	17.023
CHT2-1A-9	1.477	4.470	0.814	0.479	1856	13	10.007
	1.056	5.930	0.221	1.761	554	10	9.435
	1.780	5.260	0.285	1.367	600	9	11.189
	0.982	5.670	0.215	1.818	566	11	8.934
	0.905	18.890	0.478	0.816	515	4	21.885
	0.608	3.500	0.370	1.055	1496	18	5.693
	1.513	4.160	0.847	0.461	1949	13	9.894
	1.531	4.260	0.769	0.507	1770	13	9.946
	0.938	5.240	0.209	1.868	588	11	8.363
	1.679	5.320	0.909	0.429	1797	11	11.573
CHT2-1A-17	1.419	6.260	0.276	1.414	592	9	10.984
	0.719	19.860	0.556	0.701	589	4	22.252
	0.312	18.040	0.461	0.847	569	5	19.077
	0.679	10.360	0.280	1.392	524	7	12.610
	0.206	2.120	0.053	7.371	447	33	2.797
CHT2-1A-22	0.948	17.820	0.473	0.825	532	5	20.959
	0.601	7.750	0.771	0.506	1768	11	9.982
	0.608	7.430	0.854	0.457	1993	11	9.745
	0.787	7.120	0.810	0.481	1838	11	10.066
	0.830	16.260	0.429	0.910	532	5	19.010
	1.184	6.050	0.258	1.514	606	9	9.994
	0.535	8.240	0.893	0.437	1979	11	10.274
	0.575	7.930	0.733	0.532	1674	10	10.045
	0.485	8.060	0.228	1.709	556	10	9.668
CHT2-1A-24	0.517	8.060	0.232	1.684	558	10	9.775
	0.619	5.150	0.648	0.601	1967	15	7.502
	1.291	7.150	0.274	1.422	565	8	11.437
	0.586	5.480	0.633	0.616	1880	14	7.685
	0.586	5.430	0.585	0.667	1759	14	7.602
	0.805	5.300	0.640	0.610	1765	13	8.289
	0.302	15.810	0.402	0.971	563	6	16.812
	0.548	14.560	0.357	1.091	515	6	16.372
	0.668	19.990	0.531	0.735	562	4	22.209
	0.906	4.010	0.617	0.633	1894	16	7.423
CHT2-1A-26	0.616	3.900	0.303	1.287	1162	16	6.055
	0.496	4.450	0.461	0.846	1683	16	6.275
	0.392	5.040	0.442	0.883	1570	16	6.464
	0.769	3.790	0.514	0.758	1770	17	6.645
	2.013	5.110	0.302	1.293	600	8	11.816
	1.839	5.320	0.287	1.359	590	8	11.440

Table 3. U–Th–Pb SIMS data from a garnet-biotite gneiss (leptynite) within Chittikara Quarry, obtained using the SHRIMP II at the John de Laeter Centre for Microscopy in Perth, Australia

		Conc. (ppm)										Ages				
Spot	Type*	U	Th	$^{232}Th/^{238}U$	%com. ^{206}Pb	$^{206}Pb^{\dagger}/^{238}U$	±‡	$^{207}Pb^{\dagger}/^{235}U$	±‡	$^{207}Pb^{\dagger}/^{238}U$	±‡	$^{206}Pb^{\dagger}/^{206}Pb$	±‡	$^{207}Pb^{\dagger}/^{206}Pb$	±‡	% disconc.
I03.01 – Garnet felsic gneiss (leptynite) – Chittikara																
I03.01.1	C	413.6	183.4	0.46	0.22	0.2777	1.1372	4.7221	1.7722	0.1233	1.3593	1579.9	15.9	2004.7	24.1	27
I03.01.2	R	2457.6	184.9	0.08	0.23	0.2758	1.0680	4.5453	1.3599	0.1195	0.8418	1570.2	14.9	1949.2	15.0	24
I03.02.1	C	339.2	199.0	0.61	0.22	0.1658	7.6718	2.6099	11.5006	0.1142	8.5678	989.0	70.3	1866.7	154.6	89
I03.02.2	R	1308.4	17.1	0.01	0.02	0.2937	4.6424	4.7714	8.8144	0.1178	7.4928	1659.9	67.9	1923.7	134.3	16
I03.03.1	C	608.2	220.2	0.37	0.08	0.3756	0.8312	6.6034	3.2774	0.1275	3.1702	2055.6	14.6	2064.0	55.9	0
I03.03.2	R	836.2	20.2	0.02	0.39	0.1409	3.6398	1.8955	4.3036	0.0976	2.2964	849.5	29.0	1578.8	43.0	86
I03.04.1	C	356.1	74.7	0.22	0.38	0.2618	0.6462	4.2880	4.3803	0.1188	4.3323	1498.8	8.6	1938.4	77.5	29
I03.05.1	C	347.7	212.0	0.63	0.01	0.4066	1.4206	7.4037	1.9277	0.1321	1.3031	2199.1	26.5	2125.8	22.8	−3
I03.06.1	C	94.9	42.5	0.46	0.77	0.3794	1.2021	6.7644	3.0753	0.1293	2.8306	2073.6	21.3	2088.5	49.8	1
I03.07.1	C	514.9	287.1	0.58	0.77	0.3620	0.6215	6.4476	1.0093	0.1292	0.7953	1991.4	10.6	2087.0	14.0	5
I03.08.1	C	589.0	162.8	0.29	1.62	0.1542	2.4256	2.3310	10.6286	0.1096	10.3481	924.5	20.9	1793.2	188.4	94
I03.09.1	C	307.1	65.7	0.22	0.03	0.3146	2.2353	5.0231	5.6769	0.1158	5.2184	1763.3	34.5	1892.4	93.9	7
I03.09.2	R	1136.0	12.1	0.01	0.15	0.2063	2.8685	3.0179	4.1932	0.1061	3.0586	1209.0	31.6	1733.6	56.1	43
I03.10.1	C	187.5	106.2	0.59	0.16	0.3727	3.4052	8.0810	9.6330	0.1573	9.0111	2042.0	59.6	2426.4	152.8	19
I03.11.1	C	1144.2	466.7	0.42	0.16	0.3267	0.7806	6.4867	1.6137	0.1440	1.4123	1822.5	12.4	2275.8	24.3	25
I03.12.1	C	192.5	100.9	0.54	0.05	0.3920	0.6567	7.0449	0.7998	0.1303	0.4565	2132.1	11.9	2102.6	8.0	−1
I03.12.2	R	1680.0	12.1	0.01	22.05	0.1183	3.4828	1.7784	38.4405	0.1091	38.2824	720.6	23.7	1783.6	697.9	148
I03.13.1	C	103.5	67.0	0.67	0.87	0.2881	2.6702	4.7918	4.2466	0.1206	3.3020	1632.1	38.5	1965.5	58.9	20
I03.14.1	C	145.5	38.6	0.27	0.08	0.2280	8.5609	3.9678	11.5283	0.1262	7.7209	1324.1	102.5	2045.7	136.4	54

* C – core, R – rim; see text for explanation; † radiogenic Pb only; ‡ all errors are absolute, 1σ errors. Conc. – Concentration; % com. – % common Pb; disconc. – disconcordant.

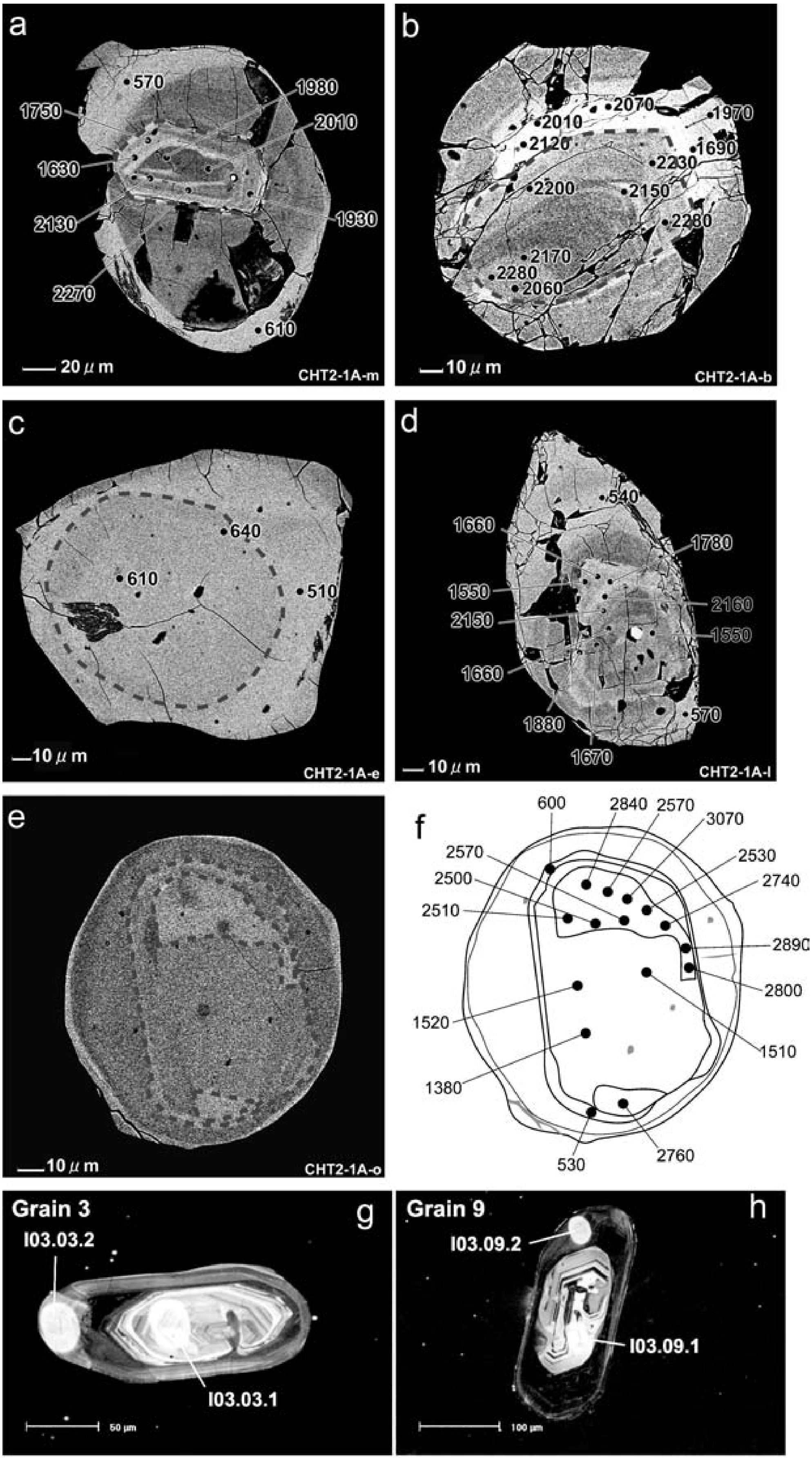
a
570
1980
1750
2010
1630
2130
1930
2270
610
20 μm
CHT2-1A-m
b
2070
1970
2010
2120
1690
2230
2200
2150
2280
2170
2280
2060
10 μm
CHT2-1A-b
c
640
610
510
10 μm
CHT2-1A-e
d
540
1660
1780
1550
2160
2150
1550
1660
570
1880
1670
10 μm
CHT2-1A-l
e
10 μm
CHT2-1A-o
f
600
2840
2570
3070
2570
2530
2500
2740
2510
2890
2800
1520
1510
1380
530
2760
Grain 3
g
I03.03.2
I03.03.1
50 μm
Grain 9
h
I03.09.2
I03.09.1
100 μm

Figure 2. For caption see facing page.

of punctuated stability of monazite in an evolving metamorphic environment (Spear & Pyle, 2002).

PbO v. ThO_2^* plots of zircons (Fig. 5) show polymodal distribution, consistent with a diverse origin. However, in the case of monazite, the PbO v. ThO_2^* plots define broad isochrons, with the cores of grains indicating an imprecise age of 1913 ± 260 Ma (Fig. 5a) with an MSWD of 0.80. The late Neoproterozoic/Cambrian cores, as well as rims, define a clear isochron (Fig. 5b) with an age of 557 ± 19 Ma (MSWD = 0.82). Compiled probability density plots of ages from zircons and monazites are shown in Figure 4. Zircons show a clustering of apparent ages between 1900 and 2300 Ma, a number of analyses with apparent Mesoproterozoic ages and a relatively precise peak at 567 ± 31 Ma. The monazite data produce a prominent late Neoproterozoic peak at 562 ± 3 Ma with some Palaeo-Mesoproterozoic apparent ages and some Cambrian apparent ages. The probability density plots bring out comparable Palaeo-Mesoproterozoic and Late Neoproterozoic/Cambrian apparent age concentrations for both Chittikara zircons and monazites.

SHRIMP U–Pb isotopic data from a Chittikara garnet–biotite gneiss (leptynite) are presented in Figure 6. The analysed zircons have very distinct highly luminescent cores and poorly luminescent rims (Fig. 2g, h). The combined core/rim data fall along an imprecise discordia line between 2106 ± 37 Ma and 524 ± 150 Ma. An evaluation of $^{207}Pb/^{206}Pb$ ages from analyses > 90 % concordant yield a weighted mean of 2099 ± 21 Ma (2σ error, MSWD = 1.5). Poorly luminescent rims have Th/U ratios < 0.1 and are amongst the most discordant analyses (Table 3, Fig. 6), suggesting these rims formed by diffusion-driven solid-state recrystallization of pre-existing zircon rather than precipitation of new zircon on a pre-existing core. The partial Pb-loss suggests that Th expulsion was more efficient than Pb expulsion during recrystallization. Combined, the data suggest that zircons within the Chittikara garnet–biotite gneiss represent one period of Palaeoproterozoic zircon formation that later partially and non-uniformly lost Pb during the late Neoproterozoic/Cambrian tectonothermal event.

5. Discussion

The blocking temperature of Pb in monazite is > 900 °C (Cherniak & Watson, 2001; Harrison, Catlos & Montel, 2002). Petrological studies and pressure–temperature computations of metapelites from Chittikara (Morimoto *et al.* 2004) indicate that the peak metamorphic temperatures exceeded 1000 °C, that is, close to the theoretical closure temperature for Pb in monazite. The incomplete resetting of monazite suggests that either the closure temperature of Pb in monazite was higher than the maximum temperature experienced by the rocks, or that robust minerals such as garnet shielded the older cores during later thermal regimes. Bindu, Yoshida & Santosh (1998) and Braun, Montel & Nicollet (1998) also observed similar cases of monazites with apparent Palaeo-Mesoproterozoic ages as well as a dominant population with late Neoproterozoic/Cambrian apparent ages.

The similarity in concordant zircon ages from the garnet–biotite gneiss (2099 ± 21 Ma) and the maximum metapelite zircon EMPA population peak (2109 ± 22 Ma) suggest that both lithologies were either sourced from the same region, or experienced the same tectonothermal event. As discussed above, the zircon morphology in the metapelite samples suggests that the cores experienced sedimentary abrasion. It therefore seems reasonable to suggest that both lithologies were deposited after Palaeoproterozoic time and were sourced from an Archaean/Palaeoproterozoic region. The younger Palaeoproterozoic and Mesoproterozoic apparent ages obtained from the metapelite may represent partial Pb loss in older zircon as seen in the garnet–biotite gneiss isotopic data. However, multiple analyses from single grains show that in many cases homogeneous older rounded cores are surrounded by younger zircon (e.g. Fig. 2c) suggesting that Pb loss may not explain all of these ~ 1900–600 Ma apparent ages and that some probably reflect Neoproterozoic zircon formation. In addition, the significant population of pre- ~ 2100 Ma EMPA apparent ages is hard to explain with a single source model, as zircons do not commonly display the extreme reverse discordance (unobservable in EMPA dating) needed to produce such a result. Instead, the most likely explanation is that these analyses represent older zircons preserved in the pelitic protolith, with heterogeneous detrital sources, whereas the more arenaceous protolith to the garnet–biotite gneiss was sourced from a single-aged terrane.

Bindu, Yoshida & Santosh (1998) were the first to analyse monazite grains from the Chittikara metapelite using the electron probe technique. In their study, they measured U, Th and Pb in two monazite grains in thin section occurring as inclusions within garnet and

Figure 2. Backscatter electron (a–e) and cathodoluminescence (g, h) images of zircons from Chittikara metapelite showing age values determined by U–Th–Pb electron probe method. The area covered by each analytical spot in the figure represents the approximate cross-sectional area of the excitation volume by the electron beam. The interpreted grain cores are shown by broken lines in (a), (b) and (c). Figure (f) is a sketch interpretation of the backscatter electron image (e) and the age values determined by the U–Th–Pb electron probe method. This grain contains the oldest cores analysed in this study mantled by successively younger rims. Figures (g, h) are cathodoluminescence images of zircons from garnet–biotite gneiss sample I03–01 from Chittikara Quarry. Bright spots are the SHRIMP analysis pits.

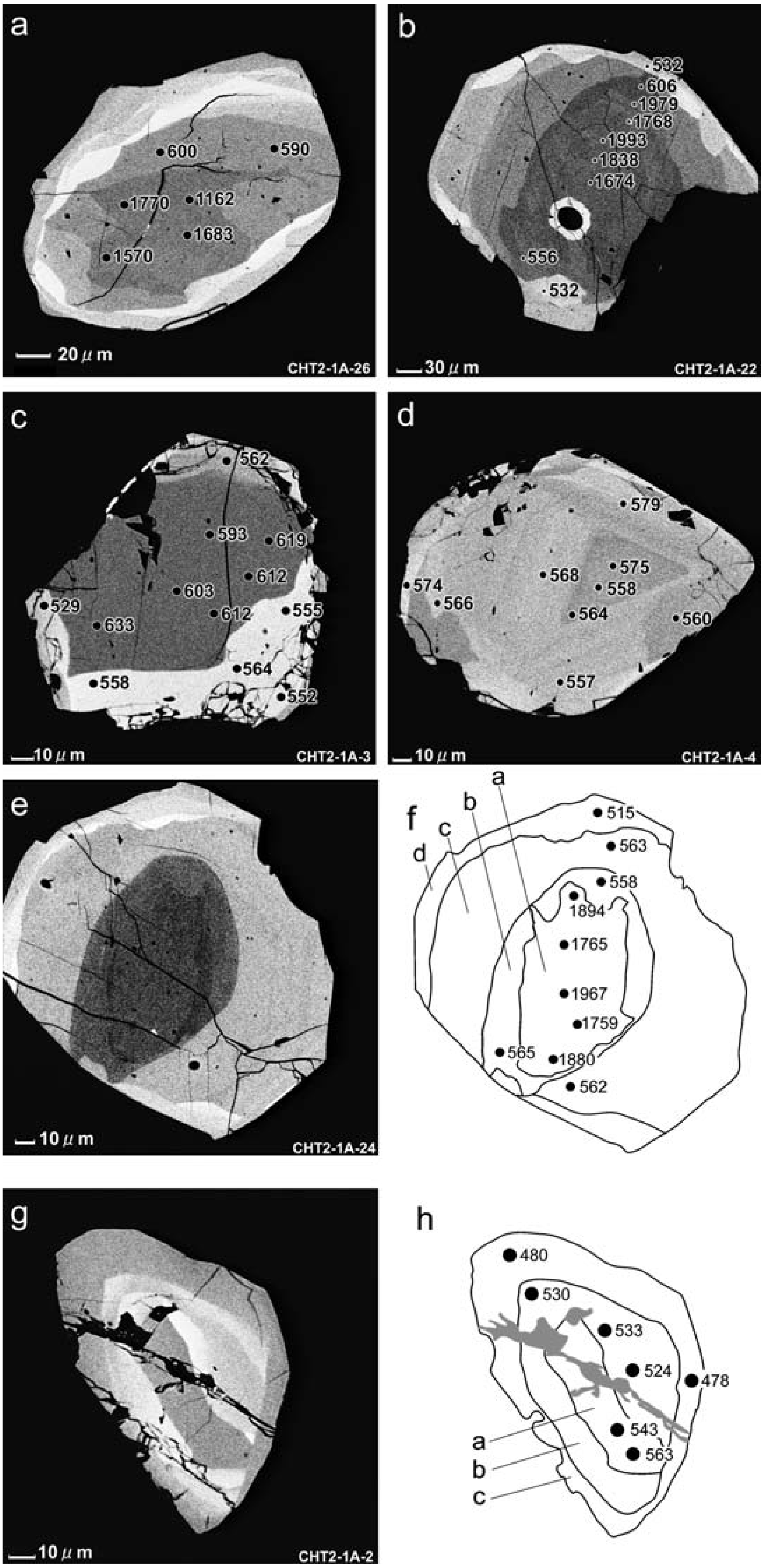
a
600
590
1770
1162
1683
1570
20 μm
CHT2-1A-26
b
532
606
1979
1768
1993
1838
1674
556
532
30 μm
CHT2-1A-22
c
562
593
619
612
603
529
633
612
555
564
558
552
10 μm
CHT2-1A-3
d
579
575
568
558
574
566
564
560
557
10 μm
CHT2-1A-4
e
10 μm
CHT2-1A-24
f
a
b
c
d
515
563
558
1894
1765
1967
1759
565
1880
562
g
10 μm
CHT2-1A-2
h
480
530
533
524
478
543
563
a
b
c

Figure 3. For caption see facing page.

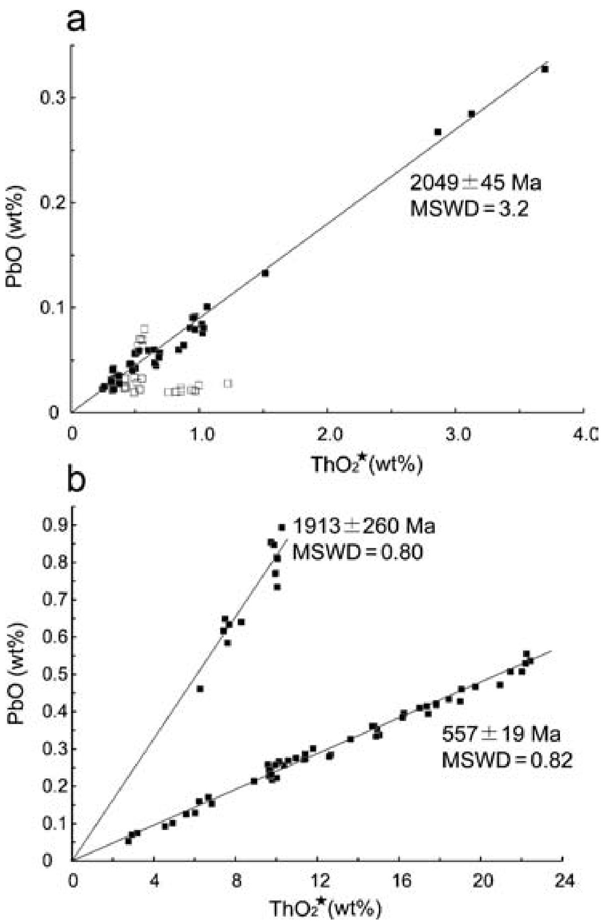

Figure 4. Probability density plots of U–Th–Pb EMPA data from the Chittikara metapelite: (a) zircons (b) monazites. Quoted ages are weighted means of data between successive peaks in the probability density plot; their associated errors are quoted at the 2 sigma level. Histogram bins are 150 Ma for zircon and 50 Ma for monazite reflecting the greater precision in the monazite analyses.

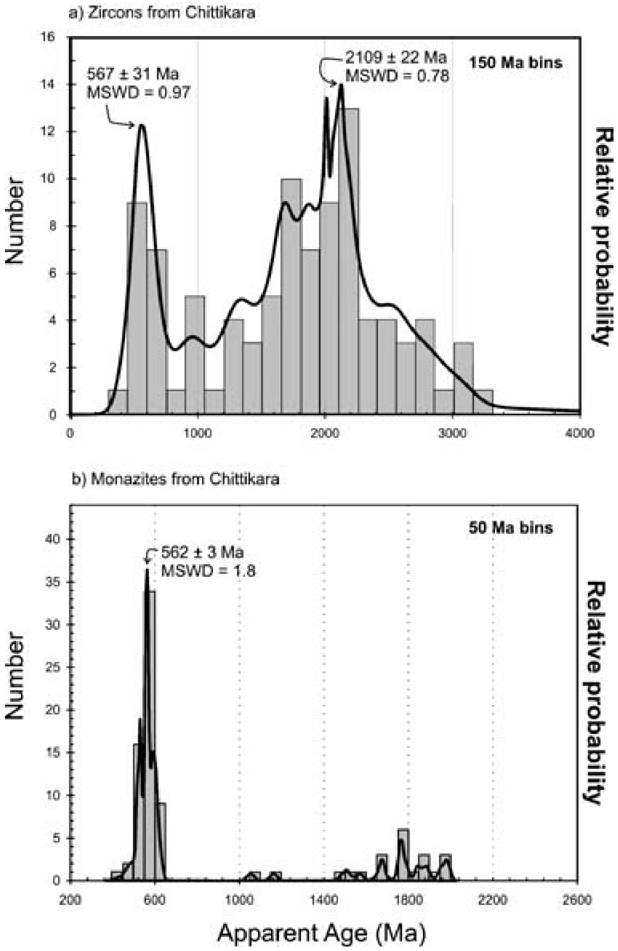

Figure 5. PbO v. ThO$_2^*$ plots of (a) zircons and (b) monazites from Chittikara metapelite. ThO$_2^*$ = function involving ThO$_2$ and UO2, required to eliminate variations in radiogenic Pb production due to variations in the Th/U ratio (Suzuki & Adachi, 1991). Indicative isochrons are plotted in (a) to illustrate a possible Palaeoproterozoic population of ages and in (b) as a reference through the diverse Palaeoproterozoic analyses and to illustrate the well-constrained age of the Neoproterozoic rims.

computed the ages from cores and rims of the grains. The ages obtained range from ~2000–1700 Ma for the cores and ~590–520 Ma for the rims. The age values obtained by Bindu, Yoshida & Santosh (1998) are identical to the results obtained from monazites in the present study (cf. Fig. 7a).

Braun, Montel & Nicollet (1998) analysed monazites from various rock types from the supracrustal belt of southern Kerala and statistical treatment of the age data revealed age populations at 1900 Ma, 580 Ma and 470 Ma. They also obtained several ages between 1700 and 800 Ma which they considered as geologically insignificant. The peak ages of the major monazite populations in the Braun, Montel & Nicollet (1998) study is closely comparable to the present results. Braun, Montel & Nicollet (1998) correlated the Palaeo-Mesoproterozoic ages with the 2000–2700 Ga Sm–Nd model ages reported by Choudhary *et al*. (1992) and Brandon & Meen (1995) and interpreted them to reflect the time of first monazite growth, concluding that this provides an upper limit for the deposition of the sedimentary protoliths of the paragneisses in southern Kerala. Braun, Montel & Nicollet (1998) and Bindu, Yoshida & Santosh (1998) did not analyse zircons. In the present study we observed that some of the zircon grains in the Chittikara metapelites are characterized by

Figure 3. Backscattered electron images of monazites from Chittikara metapelite showing age values determined by U–Th–Pb electron probe method. The area covered by each analytical spot in the figure represents the approximate cross-sectional area of the excitation volume by the electron beam. Figures (e–h) show two monazites with sketch interpretations (f, h) of the backscatter electron images (e, g) and the age values determined by the U–Th–Pb electron probe method.

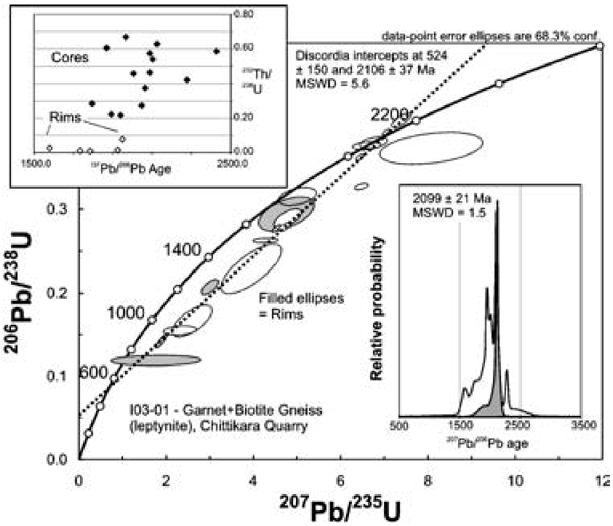

Figure 6. Concordia plot of U–Pb isotopic data from a garnet–biotite gneiss from Chittikara Quarry. Inset (top left) ^{207}Pb/^{206}Pb age versus ^{232}Th/^{238}U demonstrating the marked reduction in ^{232}Th/^{238}U ratio in the rims. Inset (bottom right) illustrates probability density plot of $>90\,\%$ concordant data (filled curve) and all data (open curve) demonstrating the dominant Palaeoproterozoic age. Discordia intercepts and quoted mean ages at 2σ error. Individual data ellipses drawn at 1σ error.

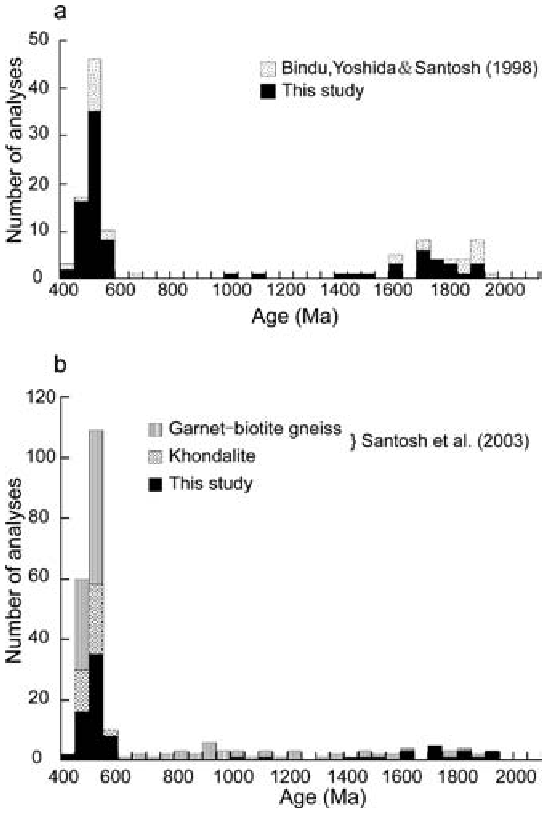

Figure 7. Histograms of age data from monazites at Chittikara compared with: (a) monazite age data from Bindu, Yoshida & Santosh (1998) and (b) Santosh *et al.* (2003).

homogeneous rounded cores with late Neoproterozoic ages (e.g. Fig. 2c, with core ages of 610–640 Ma). We interpret this to mean that sedimentation within the Trivandrum Block was as young as or later than 610 Ma. These grains have an outermost rim with Cambrian apparent ages, suggesting metamorphic overgrowth at this time.

Recently, Santosh *et al.* (2003) reported zircon and monazite U–Pb electron probe ages from the various granulite blocks in southern India, including the Trivandrum Block. We show in Figure 7b the results on monazites in garnet–biotite gneisses and metapelites analysed by Santosh *et al.* (2003) and compare these with the results reported in the present study. As seen from the histograms, both studies clearly identify the prominent 500–550 Ma peak ages, correlating with the high-grade metamorphic event in the Trivandrum Block.

Much of the high-grade metasedimentary rocks in the southern Indian/Madagascar part of Gondwana that were traditionally thought to have been deposited in Archaean or Early Proterozoic times have recently been re-interpreted as Neoproterozoic rocks based on combined SIMS U–Pb geochronology and textural analysis (de Wit *et al.* 2001; Collins *et al.* 2003; Collins & Santosh, 2004; Cox *et al.* 2004; Kinny, Collins & Razakamanana, 2004). Quartzites and garnet–biotite gneisses from the Madurai block, directly north of the Trivandrum Block preserve concordant detrital zircon cores as young as 650 ± 15 Ma that constrain deposition to be between this date and 525 ± 19 Ma, the age of metamorphic rims (Collins & Santosh, 2004). Santosh *et al.* (in press) suggested that metasedimentary rocks within the Nagercoil Granulites that form the southernmost tip of peninsular India were also Neoproterozoic and may well be lateral equivalents of Neoproterozoic southern Malagasy metasedimentary rocks. The data presented here are consistent with this correlation and suggest that: (1) the Nagercoil granulites are related to the metasedimentary rocks of the Trivandrum Block, and (2) the newly discovered Neoproterozoic metasedimentary rocks of southern India may form part of an extensive late Neoproterozoic sedimentary basin that formed during the final amalgamation of Gondwana.

Acknowledgements. M. Santosh thanks Kochi University for research facilities. SHRIMP analyses were carried out at the John de Laeter Centre for Mass Spectrometry at Curtin University and operated by a consortium consisting of Curtin University of Technology, the Geological Survey of Western Australia, and the University of Western Australia with the support of the Australian Research Council. We appreciate the assistance of Peter Kinny and Allen Kennedy during SHRIMP analysis and data reduction. Ken Ludwig is thanked for allowing the use of his programs SQUID and ISOPLOT 2.49 in data reduction and presentation. ASC's contribution forms TSRC publication no. 292. This paper contributes to IGCP projects 440 and 453.

References

Bindu, R. S., Yoshida, M. & Santosh, M. 1998. Electron microprobe dating of monazite from the Chittikara granulite, South India: evidence for polymetamorphic events. *Journal of Geosciences, Osaka City University* **41–5**, 77–83.

Brandon, A. D. & Meen, J. K. 1995. Nd isotopic evidence for the position of southernmost Indian terranes within East Gondwana. *Precambrian Research* **70**, 269–80.

Braun, I. & Kriegsman, L. M. 2003. Proterozoic crustal evolution of southernmost India and Sri Lanka. In *Proterozoic East Gondwana: Supercontinent Assembly and Breakup* (eds M. Yoshida, B. Windley and S. Dasgupta), pp. 169–202. Geological Society of London, Special Publication no. 206.

Braun, I., Montel, J. M. & Nicollet, C. 1998. Electron microprobe dating monazites from high-grade gneisses and pegmatites of the Kerala Khondalite Belt, southern India. *Chemical Geology* **146**, 65–85.

Cenki, B., Kriegsman, L. M. & Braun, I. 2002. Melt producing and melt consuming reations in the Schankovil cordierite gneisses, South India. *Journal of Metamorphic Geology* **20**, 543–61.

Chacko, T., Ravindra Kumar, G. R. & Newton, R. C. 1987. Metamorphic P–T conditions of the Kerala (South India) Khondalite Belt, a granulite facies supracrustal terrain. *Journal of Geology* **95**, 343–58.

Cherniak, D. J. & Watson, E. B. 2001. The influence of diffusion on U–Pb systematics. *11th Annual Goldschmidt Conference, Abstract* 3260.

Choudhary, A. K., Harris, N. B. W., Calsteren, P. V. & Hawksworth, C. J. 1992. Pan-African charnockite formation in Kerala, South India. *Geological Magazine* **129**, 257–64.

Collins, A. S., Kröner, A., Fitzsimons, I. C. W. & Razakamanana, T. 2003. Detrital Footprint of the Mozambique Ocean: U/Pb SHRIMP and Pb Evaporation Zircon Geochronology of Metasedimentary Gneisses in Eastern Madagascar. *Tectonophysics* **375**, 77–99.

Collins, A. S. & Pisarevsky, S. A. 2005. Amalgamating eastern Gondwana: the evolution of the Circum-Indian Orogens. *Earth-Science Reviews*, in press.

Collins, A. S. & Santosh, M. 2004. New protolith provenance, crystallisation and metamorphic U–Pb zircon SHRIMP ages from southern India. In *International Field Workshop on the Southern Granulite Terrane* (eds T. R. K. Chetty and Y. J. Bhaskar Rao), pp. 73–6. Hyderabad, India: National Geophysical Reseach Institute.

Collins, A. S. & Windley, B. F. 2002. The Tectonic Evolution of central and northern Madagascar and its place in the Final Assembly of Gondwana. *Journal of Geology* **110**, 325–40.

Compston, W., Williams, I. S. & Meyer, C. 1984. U–Pb geochronology of zircons from lunar breccia 73217 using a sensitive high mass-resolution ion microprobe. *Journal of Geophysical Research* **89** (Supplement), B525–34.

Cooper, J. A., Reynolds, P. H. & Richards, J. R. 1969. Double-spike calibration of the Broken Hill standard lead. *Earth and Planetary Science Letters* **6**, 467–78.

Cox, R., Coleman, D. S., Chokel, C. B., DeOreo, S. B., Collins, A. S., Kröner, A. & De Waele, B. 2004. Proterozoic tectonostratigraphy and paleogeography of central Madagascar derived from detrital zircon U–Pb age populations. *Journal of Geology* **112**, 379–400.

de Wit, M. J., Bowring, S. A., Ashwal, L. D., Randrianasolo, L. G., Morel, V. P. I. & Rambeloson, R. A. 2001. Age and Tectonic Evolution of Neoproterozoic ductile shear zones in southwestern Madagascar, with implications for Gondwana studies. *Tectonics* **20**, 1–45.

Harrison, T. M., Catlos, E. J. & Montel, J.-M. 2002. U–Th–Pb dating of phosphate minerals. In *Reviews in Mineralogy and Geochemistry: Phosphates, Geochemical, Geobiological and Materials Importance* (eds M. J. Kohn, J. Rakovan and J. M. Hughes), pp. 523–58. Washington: Mineralogical Society of America.

Hinthorne, J. R., Anderson, C. A., Conrad, R. L. & Lovering, J. F. 1979. Single-grain ^{207}Pb/^{206}Pb and U/Pb age determinations with a 10 μm spatial resolution using the ion microprobe mass analyser (IMMA). *Chemical Geology* **25**, 271–303.

Hoskin, P. W. O. & Black, L. P. 2000. Metamorphic zircon formation by solid-state recrystallisation of protolith igneous grains. *Journal of Metamorphic Geology* **18**, 423–39.

Kinny, P. D., Collins, A. S. & Razakamanana, T. 2004. Provenance hints and age constraints of metasedimentary gneisses of Southern Madagascar from SHRIMP U–Pb zircon data. In *International Field Workshop on the Southern Granulite Terrane* (eds T. R. K. Chetty and Y. J. Bhaskar Rao), pp. 97–8. Hyderabad, India: National Geophysical Research Institute.

Kretz, R. 1983. Symbols for rock-forming minerals. *American Mineralogist* **68**, 277–9.

Meert, J. 2003. A synopsis of events related to the assembly of eastern Gondwana. *Tectonophysics* **362**, 1–40.

Meert, J. G. & Van der Voo, R. 1997. The assembly of Gondwana 800–550 Ma. *Journal of Geodynamics* **23**, 223–36.

Montel, J. M., Foret, S., Veschambre, M., Nicollet, C. & Provost, A. 1996. Electron microprobe dating of monazite. *Chemical Geology* **131**, 37–53.

Morimoto, T., Santosh, M., Tsunogae, T. & Yoshimura, Y. 2004. Spinel + quartz association from the Kerala khondalites, southern India: evidence for ultrahigh-temperature metamorphism. *Journal of Mineralogical and Petrological Sciences* **99**, 257–78.

Nandakumar, V. & Harley, S. L. 2000. A reappraisal of the pressure–temperature path of granulites from the Kerala Khondalite Belt, Southern India. *Journal of Geology* **108**, 687–703.

Nelson, D. R. 1997. *Compilation of SHRIMP U–Pb zircon geochronology data*, 1996. Perth, Australia: Geological Survey of Western Australia.

Rubatto, D. & Gebauer, D. 2000. Use of cathodoluminescence for U–Pb zircon dating by ion microprobe: some examples from the western Alps. In *Cathodoluminescence in Geosciences* (eds M. Pagel, V. Barbin, P. Blanc and D. Ohnenstetter), pp. 373–400. Berlin: Springer-Verlag.

Santosh, M. 1987. Cordierite gneisses of southern Kerala, India: petrology, fluid inclusions and implications for crustal uplift history. *Contributions to Mineralogy and Petrology* **96**, 343–56.

Santosh, M. 1996. The Trivandrum and Nagercoil Granulite Blocks. In *The Archean and Proterozoic Terrains of southern India within East Gondwana* (eds M. Santosh and M. Yoshida), pp. 243–77. Gondwana Research

Group Memoir no. 3. Osaka: Field Science Publishers.

SANTOSH, M., JACKSON, D. H. & HARRIS, N. B. W. 1993. The significance of channel and fluid-inclusion CO_2 in cordierite: evidence from carbon isotopes. *Journal of Petrology* **34**, 233–58.

SANTOSH, M., TAGAWA, M., YOKOYAMA, K. & COLLINS, A. S. In press. U–Pb Electron Probe Geochronology of the Nagercoil Granulites, Southern India: Implications for Gondwana Amalgamation. *Journal of Asian Earth Sciences.*

SANTOSH, M. & WADA, H. 1993*a*. A carbon isotope study of graphites from the Kerala Khondalite Belt, southern India: evidence for CO_2 infiltration in granulites. *Journal of Geology* **101**, 643–51.

SANTOSH, M. & WADA, H. 1993b. Microscale isotopic zonation in graphite crystals: evidence for channelled CO_2 influx in granulites. *Earth and Planetary Science Letters* **119**, 19–26.

SANTOSH, M.,YOKOYAMA, K., BIJU-SEKHAR, S. & ROGERS, J. J. W. 2003. Multiple tectonothermal events in the granulite blocks of southern India revealed from EPMA dating: implications on the history of supercontinents. *Gondwana Research* **6**, 29–63.

SPEAR, F. S. & PYLE, J. M. 2002. Apatite, monazite and xenotime in metamorphic rocks. In *Reviews in Mineralogy and Geochemistry: Phosphates, Geochemical, Geobiological and Materials Importance* (eds M. J. Kohn, J. Rakovan and J. M. Hughes), pp. 293–336. Washington: Mineralogical Society of America.

STERN, R. J. 1994. Arc Assembly and continental collision in the Neoproterozoic East African orogeny – implications for the consolidation of Gondwana. *Annual Review of Earth and Planetary Sciences* **22**, 319–51.

STEVENS KALCEFF, M. A., PHILLIPS, M. R., MOON, A. R. & KALCEFF, W. 2000. Cathodoluminescence microcharacterisation of silicon dioxide polymorphs. In *Cathodoluminescence in Geosciences* (eds M. Pagel, V. Barbin, P. Blanc and D. Ohnenstetter), pp. 193–224. Berlin: Springer-Verlag.

SUZUKI, K. & ADACHI, M. 1991. Precambrian provenance and Silurian metamorphism of the Tsubosawa paragneiss in the South Kitakami terrane, northeast Japan, revealed by the chemical Th-U-total Pb isochron ages of monazite, zircon and xenotime. *Geochemical Journal* **25**, 357–76.

SUZUKI, K. & ADACHI, M. 1992. Middle Precambrian detrital monazite and zircon from the Hida gneiss on Oki-Dogo island, Japan: their origin and implications for the correlation of basement gneiss of Southwest Japan and Korea. *Tectonophysics* **235**, 277–92.